Supporting Information:
Late Neandertals in Southeastern Iberia:
Sima de las Palomas del Cabezo Gordo, Murcia, Spain

Michael J. Walker, Josep Gibert, Mariano V. López, A. Vincent Lombardi, Alejandro Pérez-Pérez, Josefina Zapata, Jon Ortega, Thomas Higham, Alistair Pike, Jean-Luc Schwenninger, João Zilhão, Erik Trinkaus

Supporting Information I:
The Sima de la Palomas

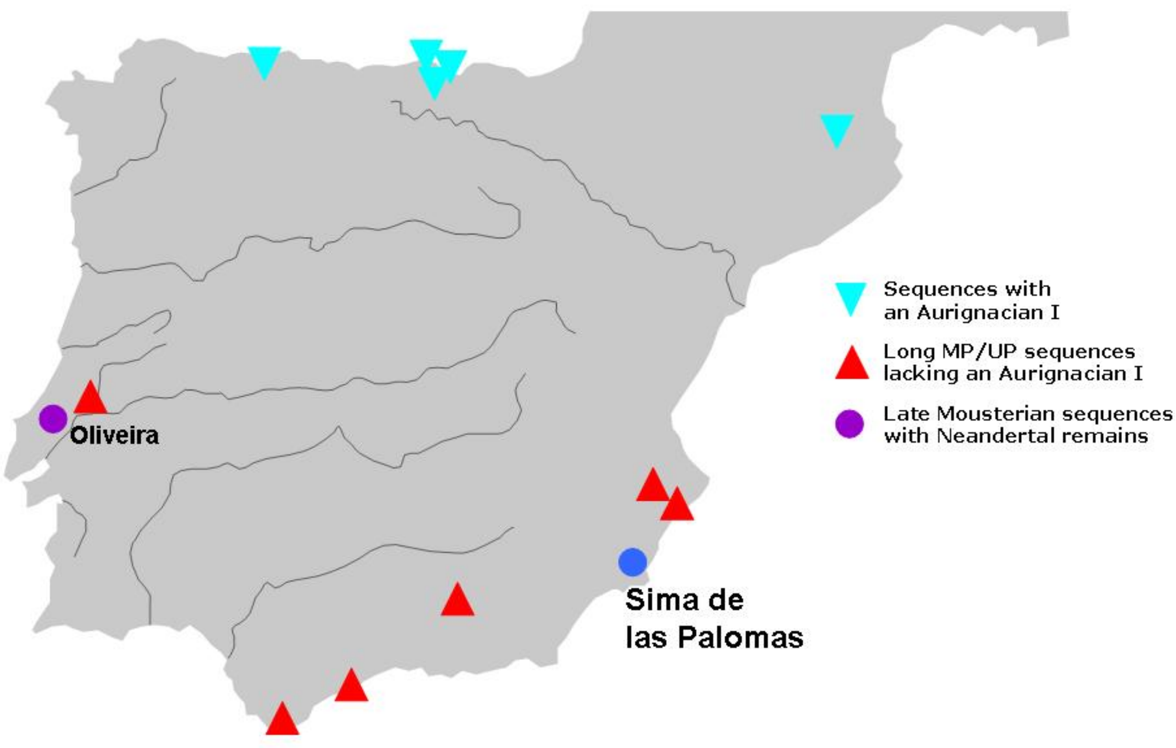

SI Figure 1. Map of Iberia with the location of the Sima de las Palomas (blue circle). The other sites include the late Neandertals from Oliveira, early Aurigiacian sites (all north of the "Ebro Frontier"), and Middle-Upper Paleolithic sites in southern Iberia that lack early Aurignacian levels.

SI Figure 2. View of the Cabezo Gordo from the Campo de Cartagena plain. The position of the Sima de las Palomas is indicated by the arrow.

SI Figure 3. View up the side of the Cabezo Gordo, with the position of the modern upper entrance of the Sima de las Palomas (covered by a protective grill) indicated.

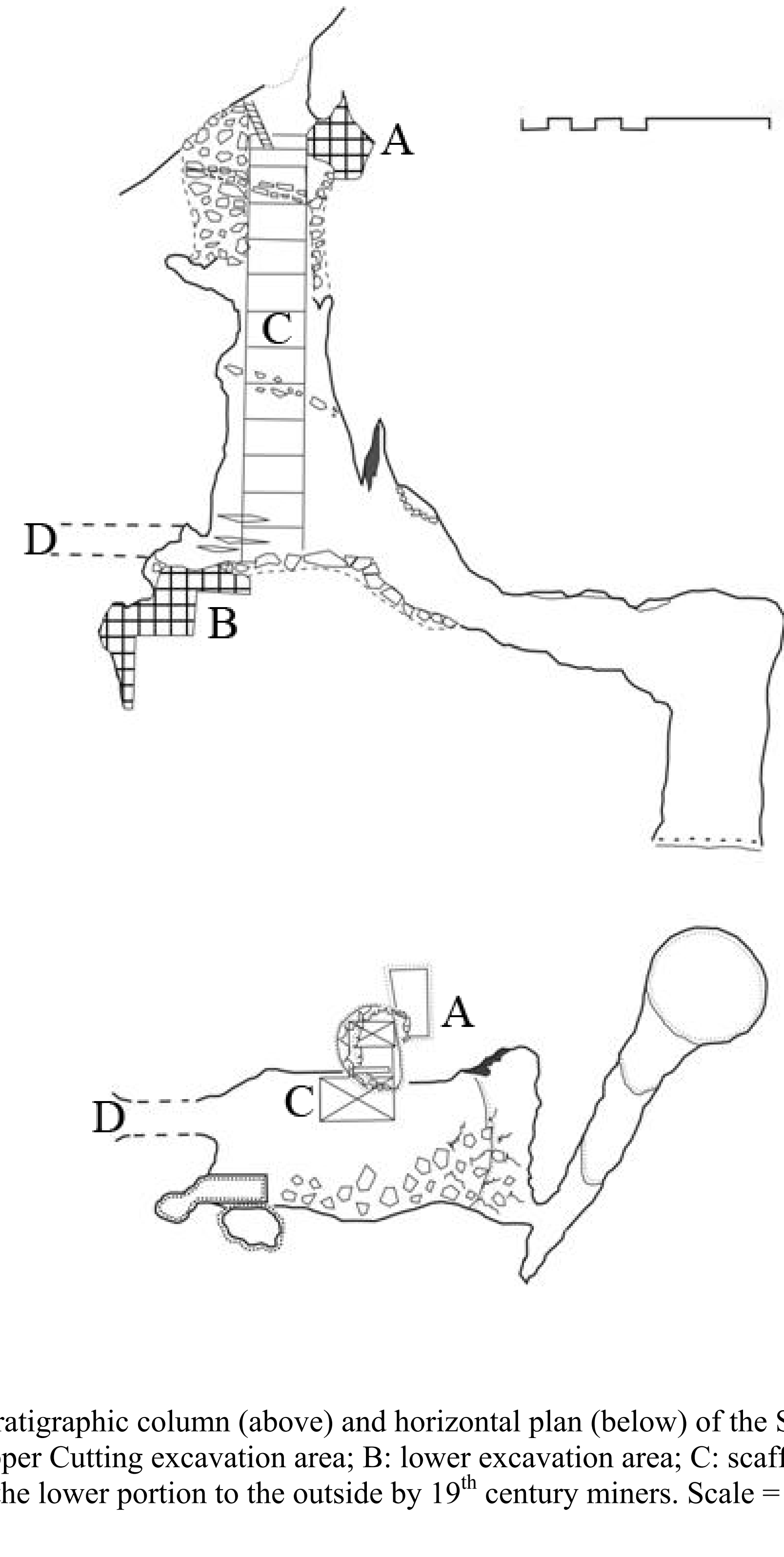

SI Figure 4. Stratigraphic column (above) and horizontal plan (below) of the Sima de las Palomas. A: Upper Cutting excavation area; B: lower excavation area; C: scaffolding; D: tunnel extended from the lower portion to the outside by 19th century miners. Scale = 10 m.

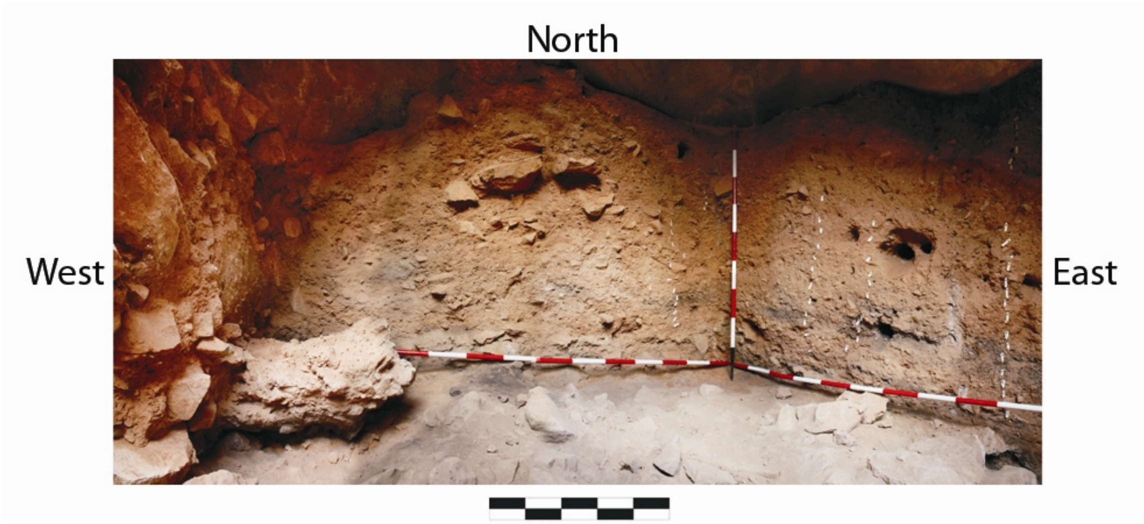

SI Figure 5. The Upper Cutting of the Sima de las Palomas at the end of the 2008 excavation season, with the west, north and east profiles. The burnt horizons are evident in the north and especially east profiles, and the éboulis is evident in the west profile. Lower scale = 1 m.

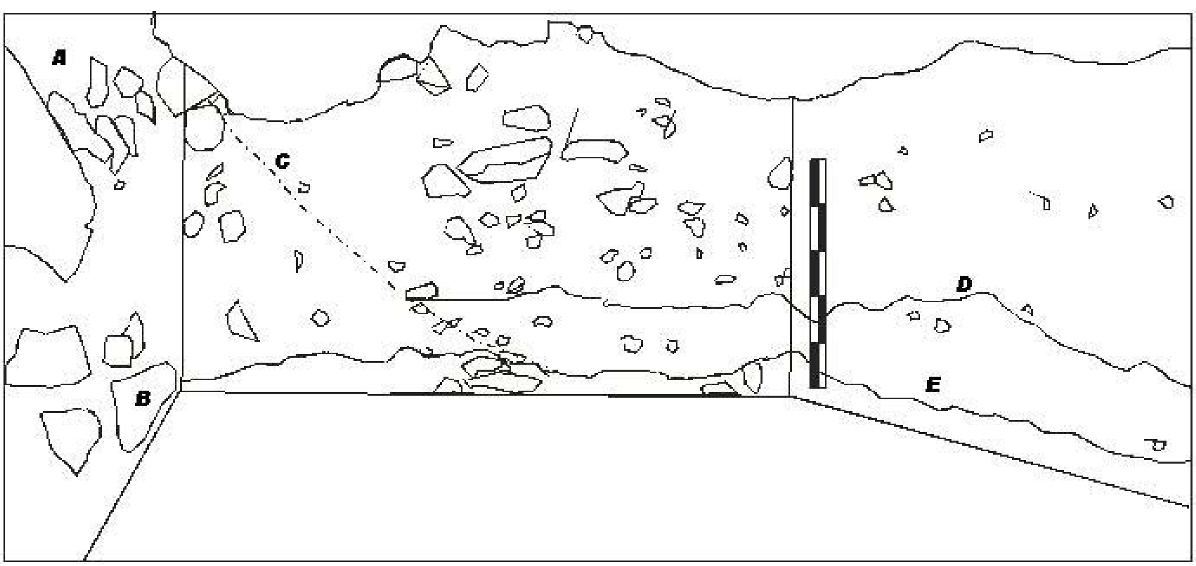

SI Figure 6. Stratigraphic rendition of the 2008 Upper Cutting profiles. A: Éboulis above the northwestern corner of the excavated cutting; B: Levels 2m-2o breccia containing human bones; C: Projection of the scree slope (éboulis) which is less perceptible in this rear profile than it had been in now removed sections parallel to it in the foreground; D: Uppermost limit (levels ~2h-2i) of lens of burnt sediment mainly in the northeastern area of the cutting; E: Lower limit of burnt ashy sediment (levels 2m-2o) in the northern and eastern area of the cutting.

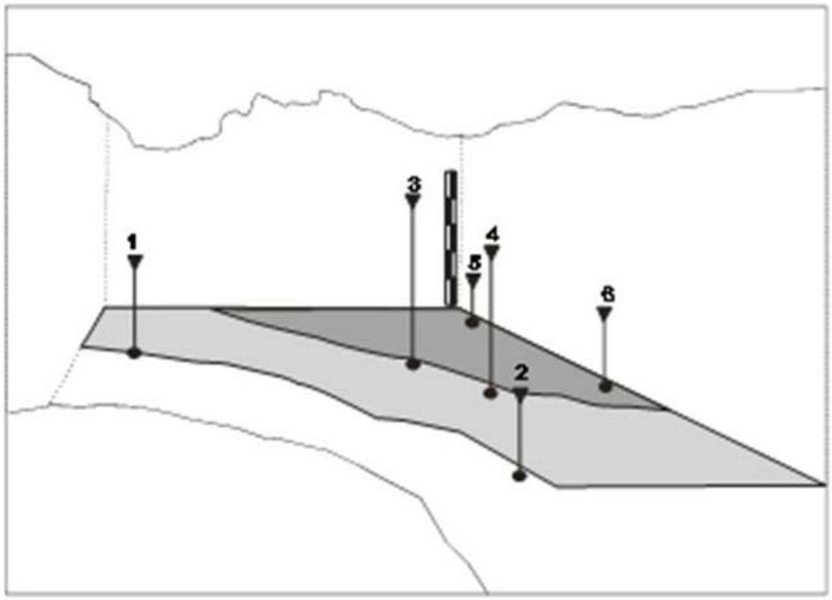

SI Figure 7. Relative positions of the burnt sediment level, a marble slab, the two more complete Palomas human mandibles, and dating samples in the Palomas Upper Cutting. Dark gray: maximum extent of fusiform lens of dark-gray burnt sediment; Light gray: lower layer of dark-gray sediment. 1: Éboulis level 2h Palomas 96 metacarpal (APSLP1); 2: Unburnt bone from level 2i (APSLP4); 3: Level 2d Palomas 80 immature mandible; 4: Level 2f Palomas 59 mandible with the ^{14}C dated burnt bone (OxA-10666) cemented to the mandibular lingual surface; 5: Levels 2k-2l flat thin marble slab with the directly overlying sediment dated by OSL (X2509); 6: Level 2l unburnt bone (APSLP6).

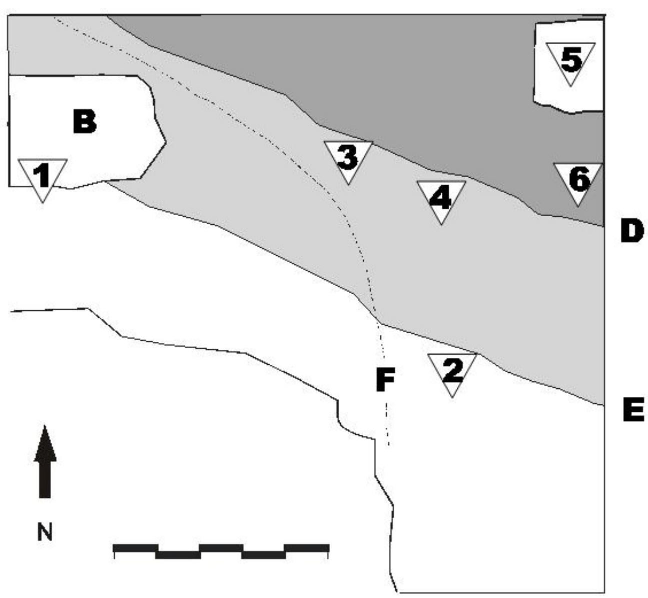

SI Figure 8. Horizontal distribution of samples and levels in the Upper Cutting of the Sima de la Palomas. Numbers and letters as in SI Figures 6 and 7. F: horizontal limit of the éboulis scree slope.

Supporting Information II: The human remains from the Sima de la Palomas del Cabezo Gordo.

SI Table 1. Sima de la Palomas human fossil inventory. Separate portions of individual specimens are listed together but given a, b, c, etc. designations. The list for Palomas (SP) 96 is incomplete, since the specimen is still in analysis. This list replaces all previous inventories (*e.g.*, ref. 1). The remains are curated in the Área de Antropología Física, Universidad de Murcia.

SP#	Old/Field #	Identification	Maturity	Provenience	Discovery Date
1a	CG-1	Maxilla right with C to M3	mature	Shaft upper breccia	1991
1b	CG-1	Maxilla left with C to M3	mature	Shaft upper breccia	1991
1c	CG-1	Mandible right with I1 to M3	mature	Shaft upper breccia	1991
1d	CG-1	Mandible left with I1, M1 to M3	mature	Shaft upper breccia	1991
2	CG-3	Occipital squamous left	mature	Hillside rubble	1992
3	CG-4	Parietal anterior right	mature	Hillside rubble	1992
4	CG-5	Parietal posterior medial left	mature	Hillside rubble	1992
5	CG-16	Parietal anterior left?	immature	Hillside rubble	1992
6	CG-6	Mandible corpus left	mature	Hillside rubble	1993
7	CG-7	Mandible mesial corpus left	immature	Mine level rubble	1993
8	CG-8	Axis (cervical vertebra 2)	immature	Hillside rubble	1993
9	CG-9	Axis (cervical vertebra 2)	mature	Hillside rubble	1993
10	CG-10	Sutural ossicle (coronal?)	mature	Mine level rubble	1993
11	CG-15	Frontal supraorbital torus right trigone	mature	Main chamber rubble	1993
12	CG-14	Frontal supraorbital torus left?	mature	Hillside rubble	1994
13	CG-17	Fibula diaphysis left	mature	Hillside rubble	1994
14	CG-18	Ulna proximal left	immature	Upper Cutting level 2b	9 July 1994
15	CG-19	Metacarpal 2 diaphysis and head right	mature	Main chamber rubble	1994
16	CG-20	Humerus diaphysis left	immature	Hillside rubble (?)	1994
17	CG-21	Humerus trochlea and epicondyle left	mature	Hillside rubbel	1994
18	CG-22	Canine mandibular left	mature	Upper Cutting level 2d	27 July 1994
19	CG-23	Incisor 1 mandibular left	mature	Upper Cutting level 2	27 July 1994
20	N1	Incisor 2 mandibular left		Upper Cutting	1994/1996
21	N2	Incisor 1 mandibular right	immature	Upper Cutting	1994/1996
22	N3	Premolar 3 mandibular left		Upper Cutting	1994/1996
23	CG-2	Mandible right from left I1 to gonion	mature	Hillside rubble	2 July 1995
24	CG-27	Incisor 1 maxillary left	mature	Hillside rubble	4 July 1995
25	CG-28	Molar deciduous 1 mandibular right	immature	Upper Cutting level 2f	4 July 1995

SI Table 1 cont.

SP#	Old/Field #	Identification	Maturity	Provenience	Discovery Date
26	CG-30	Canine mandibular right	immature	Upper Cutting level 2f	4 July 1995
27	CG-34 (1998)	Canine deciduous	immature	Hillside rubble	5 July 1995
28	CG-24	Manual distal phalanx 2-4	mature	Upper Cutting level 2g	6 July 1995
29	CG-33 (CG-35)	Molar 2 mandibular right	mature	Upper Cutting level 2h	6 July 1995
30	CG-13	Parietal posterior inferior right	mature	Hillside rubble	8 July 1995
31	CG-31	Deciduous canine mandibular left	immature	Upper Cutting level 2i	9 July 1995
32	CG-55(CG-80),#13	Humerus proximal diaphysis and epiphysis right	immature	Upper Cutting level 2i	10 July 1995
33	CG-46	Root fragment		Upper Cutting level 2i	10 July 1995
34	CG-29	Incisor 1 maxillary left	mature	Upper Cutting level 2k	17 July 1995
35	CG-26	Canine maxillary left	mature	Upper Cutting level IA	20 July 1995
36	CG-25	Molar 2 maxillary left	immature	Upper Cutting level IA	21 July 1995
37	Code 8	Incisor 2 maxillary right		Upper Cutting level IA	27 July 1995
38	CG-36 (1998)	Molar 2-3 with mandibular fragment		Upper Cutting level IB	1995/1996
39	CG-35	Deciduous incisor 1 maxillary left	immature	Upper Cutting level IA	27 July 1996
40	CG-42	Molar deciduous 1 mandibular left	immature	Upper Cutting level IA	27 July 1996
41	CG-40 (1998)	Incisor 1 mandibular right?	immature	Upper Cutting level IA	27 July 1996
42	CG-38	Molar crown and root fragment		Upper Cutting level IB	28 July 1996
43	CG-39 (1998)	Incisor 2 maxillary left	immature ?	Upper Cutting level IB	29 July 1996
44	CG-40	Canine mandibular right	mature	Upper Cutting level IB	29 July 1996
45	CG-44	Premolar 3 mandibular right	immature	Upper Cutting level IB	29 July 1996
46	CG-45	Root fragment		Upper Cutting level IB	29 July 1996
47	CG-47 (1998)	Incisor 1 mandibular right	mature	Upper Cutting level IB	29 July 1996
48	CG-37	Incisor 2 maxillary right	mature	Upper Cutting level IBa	31 July 1996
49	CG-51 (exCG-49)	Mandible corpori	immature	Upper Cutting level IA	2 August 1996
50	CG-47	Molar 1-3 mandibular right	mature ?	Hillside rubble	6 August 1996
51	CG-43	Molar 3 maxillary right with alveolus	mature	Upper Cutting level I	9 August 1996
52		Femur diaphysis left	immature	Hillside rubble	2 August 1997
53	CG-48	Premolar 4 maxillary left	mature	Upper Cutting level 2c	13 August 1997
54	CG-49	Canine mandibular right	mature	Upper Cutting level 2c	13 August 1997
55	CG-50	Root - anterior maxillary tooth	mature	Upper Cutting level 2c	15 August 1997
56	CG-68	Parietal (left?)		Hillside rubble	17 August 1997
57	Code 3, CG-65	Premolar 4 mandibular right	?mature	Upper Cutting level 2d	19 August 1997
58	Code 25, CG-71	Molar 3 mandibular right	?mature	Upper Cutting level 2d	29 July 1998

SI Table 1 cont.

SP#	Old/Field #	Identification	Maturity	Provenience	Discovery Date
59	CG-70	Mandibular body left from I2 to M3, with C-M2	mature	Upper Cutting level 2f	1 August 1998
60	Code 19, CG-72	Premolar 3 maxillary right	?mature	Upper Cutting level 2f	6 August 1998
61	Code 17, CG-73	Deciduous molar 1 right; mandibular fragment	immature	Upper Cutting level 2f	9 August 1998
62	CG-74	Frontal supraorbital torus right trigone	mature	Hillside rubble	1998
63	CG-84	Rib 1 right	immature	Hillside rubble	23 July 1999
64	CG-82	Radius diaphysis left	mature	Hillside rubble	23 July 1999
65	CG-75,#9	Manual middle phalanx 2-4	mature	Shaft scaffolding tower	9 August 1999
66	CG-76,#10	Proximal or middle phalanx 2-5	immature	Upper Cutting level 2k	31 July 2000
67	CG-98	Pedal middle phalanx	mature	Upper Cutting level IA	29 July 2001
68	Code 21, CG-92	Premolars 3 & 4 right in maxillary fragment	mature	Upper Cutting level IA	29 July 2001
69	Code 16, CG-94	Deciduous molar 2 mandibular right fragment	immature	Upper Cutting level IAc	6 August 2001
70	Code 13, CG-96	Deciduous molar 2 mandibular right	immature	Upper Cutting level IAd	6 August 2001
71	Code 22, CG-93	Deciduous molar 1 maxillary left	immature	Upper Cutting level IAd	6 August 2001
72	Code 26, CG-97	Molar 1 maxillary left fragment		Upper Cutting level IAf	8 August 2001
73	Code 23	Incisor 1 maxillary left? labial crown		Upper Cutting level IAh	25 July 2002
74	Code 12, CG-99	Canine maxillary left	mature	Upper Cutting level IAi	29 July 2002
75	Code 20, CG-100	Premolar 4 mandibular right	mature	Upper Cutting level IAe-h	9 August 2002
76	Code 4, CG-106	Premolar 3 mandibular right	mature	Upper Cutting level 2a	25 July 2003
77	CG-104	Femur head	mature	Upper Cutting level 2b	28 July 2003
78	Code 2, CG-110	Premolar 4 mandibular left		Upper Cutting level 2c	30 July 2003
79	Code 11, CG-107	Incisor 1 maxillary left		Upper Cutting level 2a	31 July 2003
80	CG-105	Mandible left with molar 2	immature	Upper Cutting level 2d	5 August 2003
81	Code 24, CG-108	Molar 1/2? mandibular left		Upper Cutting level 2b	5 August 2003
82	Code 7, CG-109	Canine mandibular left		Upper Cutting level 2b	6 August 2003
83	Code14	Deciduous molar 2 mandibular right	immature	Upper Cutting level 2c	7 August 2003
84	Code 5	Molar 1 mandibular left		Upper Cutting level 2f	10 August 2003
85	Code 18, CG-116	Deciduous incisor 2 maxillary left	immature	Upper Cutting loose dirt	10 August 2003
86		Pedal proximal phalanx 2-4	immature	Upper Cutting level 2g	23 July 2004
87	Code 1	Premolar 4 mandibular left		Upper Cutting level 2g	23 July 2004
88	Code 15	Deciduous molar 2 mandibular left with lat mand alv	immature	Upper Cutting level 2g	23 July 2004
89	Code 6	Incisor 2 mandibular right		Upper Cutting level 2m	25 July 2004
90	Code 10	Incisor 1 maxillary left		Upper Cutting level 2e	27 July 2004
91	Code 9	Incisor 2 mandibular left		Upper Cutting level 2e	27 July 2004

SI Table 1 cont.

SP#	Old/Field #	Identification	Maturity	Provenience	Discovery Date
92a	SP05H004	Cuboid left	mature	Upper Cutting level 2h	31 July 2005
92b	SP05H004	Lateral cuneiform left	mature	Upper Cutting level 2h	31 July 2005
92c	SP05H004/008	Metatarsal 1 left	mature	Upper Cutting level 2h	31 July 2005
92d	SP05H004/005/011	Metatarsal 2 left	mature	Upper Cutting level 2h	31 July 2005
92e	SP05H004/005	Metatarsal 3 left	mature	Upper Cutting level 2h	31 July 2005
92f	SP05H004/005	Metatarsal 4 left	mature	Upper Cutting level 2h	31 July 2005
92g	SP05H004	Metatarsal 5 left	mature	Upper Cutting level 2h	31 July 2005
92h	SP05H005	Pedal proximal phalanx 2 left	mature	Upper Cutting level 2h	31 July 2005
92i	SP05H005	Pedal proximal phalanx 3 left	mature	Upper Cutting level 2h	31 July 2005
92j	SP05H005	Pedal proximal phalanx 4 left	mature	Upper Cutting level 2h	31 July 2005
92k	SP05H005	Pedal proximal phalanx 5 left	mature	Upper Cutting level 2h	31 July 2005
92l	SP05H007	Pedal middle phalanx 2-4 left	mature	Upper Cutting level 2h	31 July 2005
92m	SP05H007	Pedal middle phalanx 2-4 left	mature	Upper Cutting level 2h	31 July 2005
92n	SP05H005	Pedal middle phalanx 5 left	mature	Upper Cutting level 2h	31 July 2005
92o	SP05H011	Lateral hallucal sesamoid left	mature	Upper Cutting level 2h	31 July 2005
92p	SP05H004	Medial hallucal sesamoid left	mature	Upper Cutting level 2h	31 July 2005
92q	SP05H009	Metacarpal 3 left	mature	Upper Cutting level 2h	31 July 2005
92r	SP05H009/104	Metacarpal 4 left	mature	Upper Cutting level 2h	31 July 2005
92s	SP05H009	Metacarpal 5 left	mature	Upper Cutting level 2h	31 July 2005
92t	SP05H009	Manual proximal phalanx 3 left	mature	Upper Cutting level 2h	31 July 2005
92u	SP05H009	Manual proximal phalanx 4 left	mature	Upper Cutting level 2h	31 July 2005
92v	SP05H009	Manual proximal phalanx 5 left	mature	Upper Cutting level 2h	31 July 2005
92w	SP05H009	Manual middle phalanx 3 left	mature	Upper Cutting level 2h	31 July 2005
92x	SP05H009	Manual middle phalanx 4 left	mature	Upper Cutting level 2h	31 July 2005
92y	SP05H009	Manual distal phalanx 3 left	mature	Upper Cutting level 2h	31 July 2005
92z	SP05H013	Metacarpal 2 head right	mature	Upper Cutting level 2h	1 August 2005
92aa	SP05H100	Trapezius left	mature	Upper Cutting level 2h	4 August 2005
92bb	SP05H100	Trapezoid left	mature	Upper Cutting level 2h	4 August 2005
92cc	SP05H020	Metacarpal proximal epiphysis	mature	Upper Cutting level 2h	1 August 2005
92dd	SP05H021/SP05H032	Metacarpal proximal epiphysis and diaphyisis	mature	Upper Cutting level 2h	1 August 2005
92ee	SP05H104	Metacarpal 4 head left	mature	Upper Cutting level 2h	4 August 2005

SI Table 1 cont.

SP#	Old/Field #	Identification	Maturity	Provenience	Discovery Date
92ff	SP05H016	Humerus distal right	mature	Upper Cutting level 2h	1 August 2005
92gg	SP05H016	Ulna proximal right	mature	Upper Cutting level 2h	1 August 2005
92hh	SP05H016	Ulna distal right	mature	Upper Cutting level 2h	1 August 2005
92ii	SP05H016	Radius proximal right	mature	Upper Cutting level 2h	1 August 2005
92jj	SP05H016	Triquetral right	mature	Upper Cutting level 2h	1 August 2005
92kk	SP05H016	Pisiform right?	mature	Upper Cutting level 2h	1 August 2005
92ll	SP05H036	T12 thoracic verterbra	mature	Upper Cutting level 2h	1 August 2005
92mm	SP05H002/071B	Femur proximal diaphysis and trochanters right	mature	Upper Cutting level 2h	29 July, 4 Aug 2005
92nn	SP05H014	Femur distal diaphysis with lateral condyle right	mature	Upper Cutting level 2h	1 August 2005
92oo	SP05H071A/107	Femur prox to mid-diaph and trochanters left	mature	Upper Cutting levels 2h/2k	4, 7 August 2005
92pp	SP05H010	Pelvic fragment	mature	Upper Cutting level 2h	31 July 2005
92qq	SP05H040	Pelvic fragment	mature	Upper Cutting level 2h	1 Agoust 2005
93	Code 27	Deciduous canine maxillary right	immature	Upper Cutting level 2n	27 July 2006
94	Code 29	Premolar 4 maxillary left	immature	Upper Cutting level 2o	27 July 2006
95	Code 28	Deciduous canine mandibular left	immature	Upper Cutting level 2o	28 July 2006
96a	C-K,C-B,C-D	Tibia left	mature	Upper cutting level 2e	12 October 2006
96b	C-K,C-F,C-N,C-E,C-G	Fibula left	mature	Upper cutting level 2e	12 October 2006
96c	C-A, C-H, C-O, C-K	Femur left	mature	Upper cutting level 2e	12 October 2006
96d	C-H, C-P, C-L, C-E	Femur right	mature	Upper cutting level 2e	12 October 2006
96e	C-I, C-H	Ox coxae right	mature	Upper cutting level 2e	7 August 2007
96f	C-A, C-M, C-H	Ischium and pubic arch left	mature	Upper cutting level 2e	12 October 2006
96g	C-C, C-J	Sacrum	mature	Upper cutting level 2e	12 October 2006
96h	C-f, C-d, C-ah, C-ai	Scapula right	mature	Upper cutting level 2e	9 August 2007
96i	C-f, C-d	Rib 2 right	mature	Upper cutting level 2e	10 August 2007
96j	C-f, C-d	Rib 3 right	mature	Upper cutting level 2e	10 August 2007
96k	C-f, C-d	Rib 4 right	mature	Upper cutting level 2e-2d	10 August 2007
96l	C-f, C-d	Rib 5 right	mature	Upper cutting level 2e-2d	10 August 2007
96m	C-f	Rib 6 right	mature	Upper cutting level 2e-2d	11 August 2007
96n	C-f	Rib 7 right	mature	Upper cutting level 2e-2d	11 August 2007

SI Table 1 cont.

SP#	Old/Field #	Identification	Maturity	Provenience	Discovery Date
96o	C-d, C-ai	Clavicle right	mature	Upper cutting level 2e-2d	9 August 2007
96p	C-f, C-g	Humerus right	mature	Upper cutting level 2e-2d	10 August 2007
96q	C-f, C-g	Ulna right	mature	Upper cutting level 2e-2d	10 August 2007
96r	C-f, C-g	Radius right	mature	Upper cutting level 2e-2d	10 August 2007
96s	C-t	Scaphoid right	mature	Upper cutting level 2d	11 August 2007
96t	C-f	Metacarpal 1 right	mature	Upper cutting level 2d	11 August 2007
96u	C-f, C-s	Metacarpal 2 right	mature	Upper cutting level 2d	11 August 2007
96v	C-f, C-s	Metacarpal 3 right	mature	Upper cutting level 2d	11 August 2007
96w	C-s, C-t	Metacarpal 4 right	mature	Upper cutting level 2d	11 August 2007
96x	C-s	Metacarpal 5 right	mature	Upper cutting level 2d	11 August 2007
96y	C-f	Manual proximal phalanx 1 right	mature	Upper cutting level 2d	11 August 2007
96z	C-s	Manual proximal phalanx 2 proximal epiphysis right	mature	Upper cutting level 2d	11 August 2007
96aa	C-s	Manual proximal phalanx 3 right	mature	Upper cutting level 2d	11 August 2007
96bb	C-s	Manual proximal phalanx 4 right	mature	Upper cutting level 2d	11 August 2007
96cc	C-s	Manual middle phalanx 2 right	mature	Upper cutting level 2d	11 August 2007
96dd	C-s	Manual middle phalanx 3 right	mature	Upper cutting level 2d	11 August 2007
96ee	C-s	Manual middle phalanx 4-5 right	mature	Upper cutting level 2d	11 August 2007
96ff	C-r	Manual middle phalanx 4-5 right	mature	Upper cutting level 2d	11 August 2007
96gg	C-s	Manual distal phalanx right	mature	Upper cutting level 2d	11 August 2007
96hh	C-s	Manual distal phalanx right	mature	Upper cutting level 2d	11 August 2007
96ii	C-k, C-ah, C-f	Humerus left	mature	Upper cutting level 2e-2d	10 August 2007
96jj	C-f, C-ae	Radius left	mature	Upper cutting level 2e-2d	11 August 2007
96kk	C-f, C-s	Ulna left	mature	Upper cutting level 2e-2d	11 August 2007
96ll	C-s	Scaphoid left	mature	Upper cutting level 2d	11 August 2007
96mm	C-f	Carpal right	mature	Upper cutting level 2d	11 August 2007
96nn	C-s	Carpal left	mature	Upper cutting level 2d	11 August 2007
96oo	C-ae	Carpal left	mature	Upper cutting level 2d	11 August 2007
96pp	C-ae	Carpal left	mature	Upper cutting level 2d	11 August 2007
96qq	C-ae	Carpal left	mature	Upper cutting level 2d	11 August 2007
96rr	C-w	Metacarpal left	mature	Upper cutting level 2c	10 August 2007
96ss	C-u	Metacarpal head left	mature	Upper cutting level 2c	10 August 2007
96tt	C-u, Cy	Metacarpal head left	mature	Upper cutting level 2c	10 August 2007
96uu	C-aa	Metacarpal head left	mature	Upper cutting level 2c	10 August 2007

SI Table 1 cont.

SP#	Old/Field #	Identification	Maturity	Provenience	Discovery Date
96vv	C-z	Manual proximal phalanx left	mature	Upper cutting level 2c	10 August 2007
96ww	C-z	Manual proximal Phalanx left	mature	Upper cutting level 2c	10 August 2007
96xx	C-u	Manual proximal phalanx proximal epiphysis left	mature	Upper cutting level 2c	10 August 2007
96yy	C-u	Manual middle phalanx 2-4 left	mature	Upper cutting level 2c	10 August 2007
96zz	C-z	Manual middle phalanx 2-4 left	mature	Upper cutting level 2c	10 August 2007
96aaa	C-ab	Manual middle phalanx 5 left	mature	Upper cutting level 2c	10 August 2007
96bbb	C-y	Manual distal phalanx left	mature	Upper cutting level 2c	10 August 2007
96ccc	C-ac	Manual distal phalanx left	mature	Upper cutting level 2c	10 August 2007
96ddd	C-k	Thoracic vertebra	mature	Upper cutting level 2d	10 August 2007
96eee	C-k	Thoracic vertebra	mature	Upper cutting level 2d	10 August 2007
96fff	C-k	Thoracic vertebra	mature	Upper cutting level 2d	10 August 2007
96ggg	C-i	Thoracic vertebra	mature	Upper cutting level 2e	6 August 2007
96hhh	C-i	Thoracic vertebra	mature	Upper cutting level 2e	6 August 2007
96iii	C-at	Hemimandible right	mature	Upper cutting level 2c	9 August 2007
96jjj	C-at	Mandible ramus left	mature	Upper cutting level 2c	9 August 2007
96kkk	C-at	Temporal left	mature	Upper cutting level 2c	9 August 2007
96lll	C-a, C-at	Cranial vault fragments; isolated teeth	mature	Upper cutting level 2c	9 August 2007

Supporting Information III: Radiocarbon Dating of the Sima de las Palomas

Two samples of burnt animal bone were dated at the Oxford Radiocarbon Accelerator Unit, University of Oxford. We detached by drilling a featureless fragment of burnt animal bone that had been cemented to the lingual surface of the unburnt Palomas 59 Neandertal mandibular corpus (OxA-10666). This fragment was dated along with a further determination subsequently obtained from a burnt rabbit bone (OxA-15423).

Burning significantly reduces the protein content of bone, making excessively burnt material impractical to date by targeting collagen. Burning is an important influence on the degradation of bone and its susceptibility to contamination. It also influences the interpretation one can place on relative stable N and C isotope values; the C:N ratio almost always goes higher than the standard range for fresh collagen of 2.9 to 3.5 (2); since collagen is removed and the nitrogen is only in the collagen, proportionately more carbon is present. Alteration to the $\delta^{13}C$ value is apparent even in bones that are only slightly burnt, possibly due to increased exposure to contamination or differential loss of amino acids in the collagen. The material isolated for dating is often only approximately characterizable. Usually, it is characterized simply as carbonaceous material insoluble in acid or alkali, and it consists largely of pyrolised collagen which is often further degraded and subject to post-depositional leaching. It is sometimes difficult, in cases where the carbon content is low, to rule out sediment-derived carbon contamination. Comparison of the $\delta^{13}C$ values of the extracted carbon with the values expected for bone collagen and sediment carbon is one way to assess the possibility of gross error.

Both bone fragments from Sima de las Palomas were crushed and pretreated using an acid-base-acid sequence, which is the standard treatment for charcoal at ORAU, prior to AMS dating. For OxA-10666, the insoluble residue comprised 5.3% of the total weight of the original sample and contained 8.0% carbon when combusted. The AMS radiocarbon result obtained was 34,450 ± 600 (OxA-10666). The $\delta^{13}C$ value of –21.0‰ is consistent with collagen-derived carbon, implying >75% of the carbon dated is from the bone. Sediment-derived carbon cannot be ruled out; it is most likely to have an age similar to that of the bone in which it as deposited, though it could be younger or older. There is, therefore, a possibility that the bone is older than measured, because a small amount of younger carbon would have a disproportionate effect on the age. The C:N atomic ratio of 6.9 is higher than the range for fresh bone, but this is not unexpected given the burning of the sample.

A similar situation applies to OxA-15423. However, the combustion yield (%C) indicates that this sample is composed of much higher amounts of carbon than OxA-10666. There are two possibilities. First, the sample is composed of a majority of plant-derived carbon. This is considered less likely, since there is a significant proportion of nitrogen in the sample, which is not expected from plant matter, and therefore a low C:N atomic ratio closer to collagenous values was obtained. Second, the bone is partially pyrolyzed, and there is a higher proportion of collagenous material than usually expected. The analytical data are consistent with this conclusion. The $\delta^{13}C$ value is more indicative of collagen-derived carbon. Taken together, the results provide increased confidence in the results being finite and not underestimates of age. The consistency in the two ages is a further measure of the probable finite nature of these dates.

In the absence of an agreed calibration curve for the period before 26,000 cal BP, we compared our results against the Cariaco Basin dataset, Cariaco06 (3). It provides 95% confidence intervals for the dates of 40,950 to 37,622 cal BP for OxA-10666 and 40,986 to 38,850 cal BP for OxA-15423. Alternative comparisons [Fairbanks0107 (4) and quickcal2007 1.5 (www.calpal.de)] provide statistically indistinguishable mean age estimates.

SI Table 2. Radiocarbon results and associated analytical data for the burnt bone samples from Sima de las Palomas. %Yield is the percentage yield of material resulting after the chemical pre-treatment of the samples, whose starting weight is listed in the Used column in milligrams. %C is the carbon yield upon combustion. $\delta^{13}C$ is reported with respect to VPDB and expressed in a per mille scale. C:N is the atomic ratio of carbon to nitrogen. Values were measured using an IRMS operating in continuous flow mode using a He gas.

	OxA-10666	**OxA-15423**
Material	charred faunal bone	charred rabbit bone
Used (mg)	740.0	257.1
Yield (mg)	39.25	6.30
% Yield	5.3	2.5
% C	8.0	40.9
$\delta^{13}C$	–21.0‰	–22.3‰
C:N	6.9	5.8
^{14}C Age BP	34,450 ± 600	35,030 ± 270

Supporting Information IV:
Uranium-Series Dating of Bones from the Sima de las Palomas

Bone is an open system with respect to uranium, and therefore the calculation of a U-series date from measured U-series isotopes requires a model of uranium uptake (or loss). We use the Diffusion-Adsorption (D-A) model to account for uranium uptake in bone (5). The D-A model predicts the spatial distributions ('profiles') of uranium and U-series isotopes across a bone section as uranium is taken up by the bone. It predicts that, under constant geochemical conditions, ∪-shaped uranium profiles will develop that gradually flatten over time as the bone equilibrates with the uranium in the groundwater of the burial environment. At equilibrium, the profile is uniform and uranium ceases to be incorporated into the bone. Under constant geochemical conditions, diffusion of uranium from the outer surfaces of the bone into the center leads to a ∪-shaped distribution of apparent dates, with the closed system date (i.e., the U-series date calculated assuming no uptake or loss of uranium) at the surfaces of the bone approximating the true age of the sample, and with underestimated apparent dates towards the centre (SI Figs. 9 and 10). Pike et al. (6-8) have shown that for bones where the profiles indicate uranium uptake has proceeded under relatively constant conditions, the D-A model can be used to calculate an open system date. Bone for which U-series dates have been calculated successfully using this method,

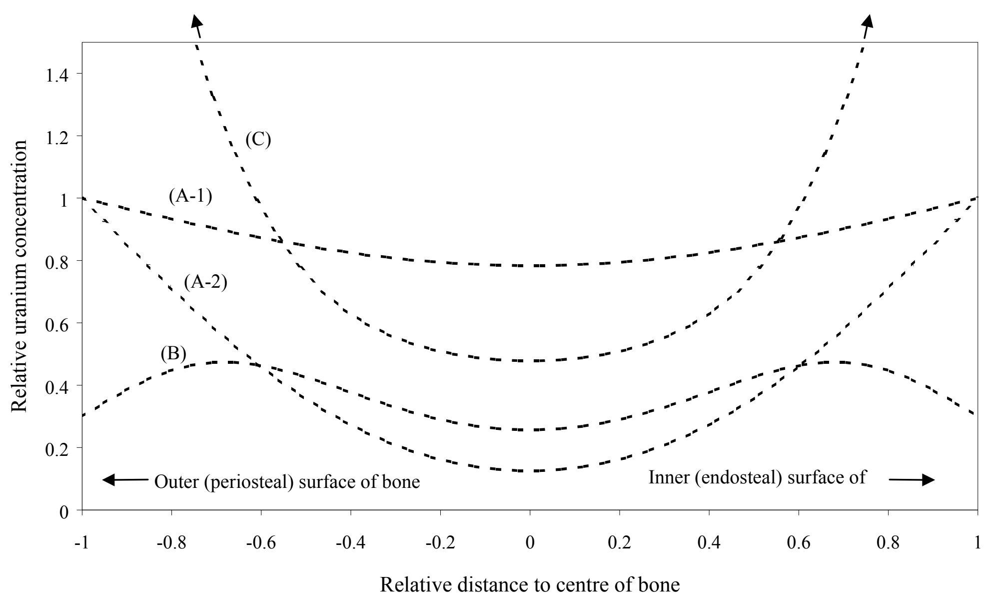

SI Figure 9. U concentration profiles across a transverse section of bone predicted by the D-A model for different uptake regimes. Shown here are U concentration profiles predicted for diffusive uptake under constant conditions with the bone nearing equilibrium with the ground water (A-1); diffusive uptake under constant conditions with the bone far from equilibrium (A-2); leaching of uranium after initial uptake (B); and a recent increase in the uptake of uranium, 'recent uptake' (C). From Eggins et al. (9)

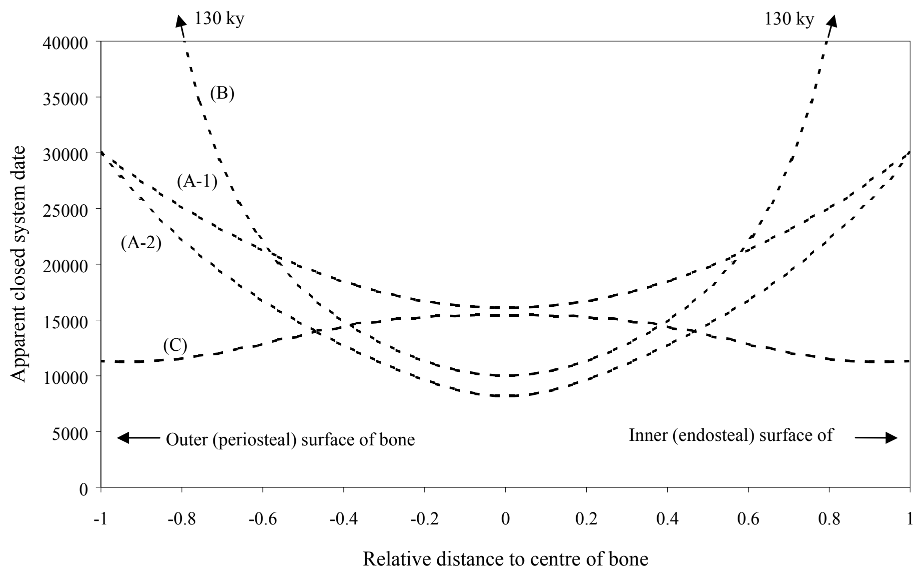

SI Figure 10. Date profiles for a 30 ky bone predicted by the D-A model for the uptake regimes shown in Fig. 1. Diffusive uptake under constant conditions (A-1) shows apparent closed system dates decreasing towards the centre of the bone section, although dates are not as underestimated as for bones further from equilibrium with the groundwater (A-2). The leaching of U after initial uptake increases the ^{230}Th/U giving over-estimated apparent closed-system dates (B). Recent increased uptake of U (C) gives underestimated apparent closed-system dates, and can lead to a characteristic ∩ distribution of dates. From Eggins et al. (9)

typically have ∪-shaped or uniform U concentration profiles, and a ∪-shaped distribution of apparent closed system U-series dates. Bones with irregular profiles, or profiles indicative of the leaching of uranium (∩, or M shaped) are rejected as unsuitable for dating.

U-series dating was attempted for several bones from the Sima de las Palomas using laser ablation multicollector plasma mass spectrometry (LA-ICP-MS). Bones were sectioned using a diamond disc, ultrasonically cleaned, dried overnight in an oven, and mounted in putty on a teflon disc and placed in the laser cell. U-series isotopes were measured on a Finnigan Neptune multi-collector ICP-MS with a 193 nm ArF Excimer laser. The laser spot size was 90 µm, and the sample traversed at 0.5 mm/min with a repetition rate of 10 Hz to ablate a track from the outer to the inner surface of the bone section. Bone sections, with isotopes previously measured using TIMS were used as calibration standards (for further details, see refs 7-9).

The measured profiles are shown in SI Figs. 11-13, and sample information is in SI Table 3. All profiles show near uniform uranium concentration and U-series date profiles, which is indicative of the bones having reached equilibrium with the burial environment relatively rapidly. Rapid equilibrium can occur in bones that are diagenetically altered. Bone porosity increases the rate of diffusion, and at the same time the partition coefficient of uranium between the groundwater and the bone reduces as the internal surface area of the bone decreases through the loss or growth of the smallest bone mineral crystals (5). Under constant conditions, rapidly equilibrated bones can approximate to a closed system, since at equilibrium U uptake ceases. We have calculated whole bone closed system dates by integrating the U-series isotopes across the profiles (SI Table 3). However, these dates must be treated as of unknown accuracy, since a change in the geochemistry of the burial environment will result in the bone rapidly re-equilibrating, which may include further uptake of uranium (leading to underestimated apparent dates) or the loss of uranium (leading to older apparent dates). Normally these phenomena can be identified by the characteristic shape of the uranium profiles as the bone re-equilibrates (SI Figs. 9 and 10). If equilibrium is too rapid, however, evidence of gain or loss of uranium is not apparent.

SI Table 3. Closed system U-series dates on bone from Palomas. Errors given at 2σ. The dates were calculated by integration of the total U-series isotopes across a profile of a transverse section of bone from outer to inner surface. One bone with irregular profiles has been excluded.

Lab number	Sample	^{230}Th/^{238}U	^{234}U/^{238}U	^{230}Th/^{232}Th	Closed system date (ka cal BP) (mean ± 2σ)
APSLP1	SP 96rr metacarpal	0.451 ± 0.049	1.1394 ± 0.0021	>100	54.1 ±7.7
APSLP4	Level 2i fauna	0.3667 ± 0.0096	1.1003 ± 0.0079	>100	43.8 ± 1.5
APSLP6	Level 2l fauna	0.401 ± 0.015	1.0655 ± 0.0086	>100	51.0 ±2.5

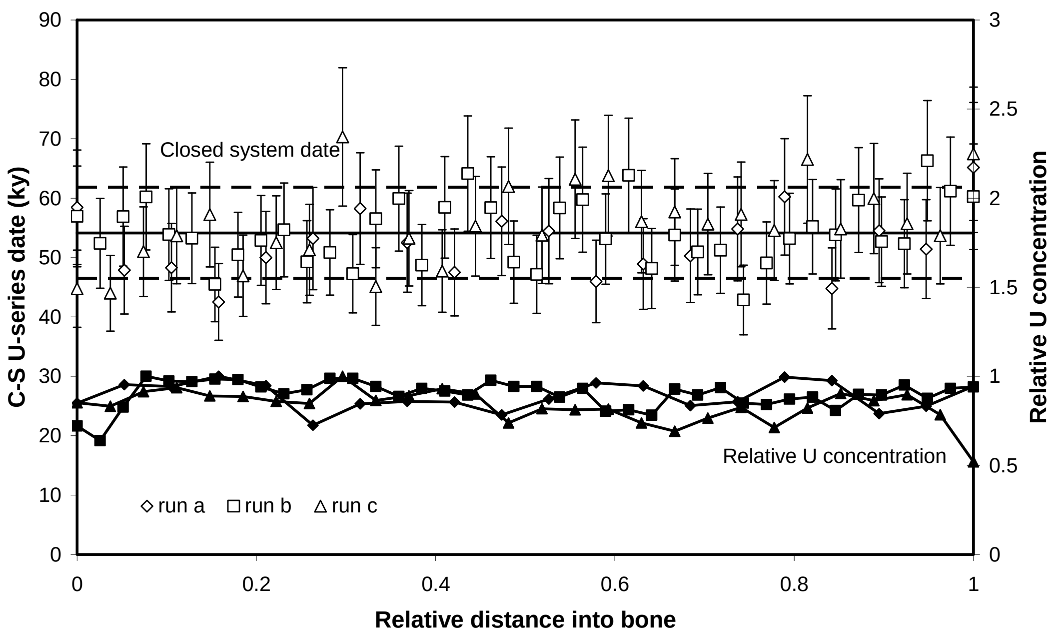

SI Figure 11. U-series and U concentration profile of APSLP1. The profiles were measured three times. The solid and broken lines represent the closed system date and uncertainty calculated from the combined data.

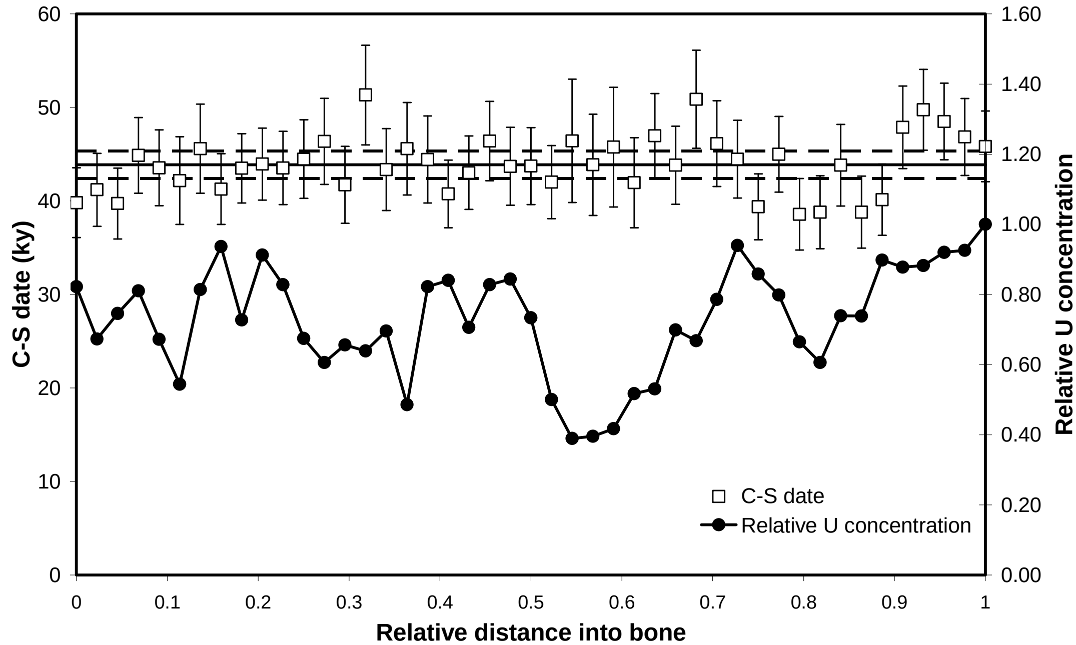

SI Figure 12. U-series and U concentration profile of APSLP4.

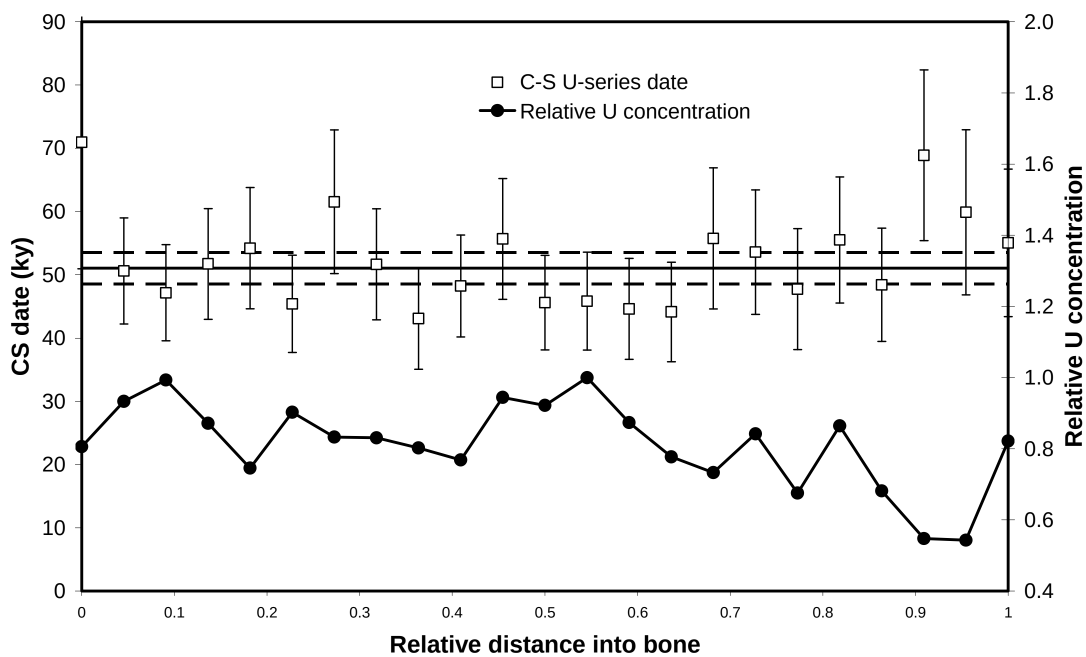

SI Figure 13. U-series and U concentration profile of APSLP6

Supporting Information V:
Optically Stimulated Luminescence Dating

Optically stimulated luminescence (OSL) dating provides an estimate of the time elapsed since luminescent minerals were last exposed to sunlight (10,11) and optical dating of sedimentary quartz has become a well established technique within Quaternary science (12,13). Light-shielded grains may accumulate charge from the effects of the environmental radiation flux to which they are exposed, and the dose received by the sample, also referred to as the paleodose, can be measured using the luminescence signal. A burial age estimate is obtained by dividing the palaeodose by the environmental dose rate.

A bloc sample weighing ≈1.5 kg was collected from the top of layer 2k for optical dating. All sample preparations took place at the Research Laboratory for Archaeology and the History of Art, University of Oxford under low intensity safe-lighting provided by filtered sodium lamps emitting at 588 nm. Laboratory procedures were designed to yield sand-sized (180-250 µm) grains of quartz for optical dating according to standard preparation methods, including the removal of the outer parts of the sample, followed by wet sieving, HCl acid digestion, density separation and etching in 68% HF acid to dissolve feldspar minerals and remove the outer 6-8 µm alpha-dosed layer.

OSL measurements were conducted using an automated system (Risø TL/OSL-DA-12 reader) and are based on a conventional single-aliquot regeneration (SAR) measurement protocol (14). Multi-grain aliquots were stimulated using 15 mW cm^{-2} of green-plus-blue (420–550 nm) light from a filtered tungsten-halogen lamp for 100 s at 125°C. The natural and regenerative doses were preheated at 260°C for 10 s, and the test doses (which are used to correct for any sensitivity changes) were preheated at a reduced temperature of 240°C for 10 s before optical stimulation. The ultraviolet OSL emission at ≈370 nm was detected using an Electron Tubes Ltd 9235QB photomultiplier tube fitted with 7.5 mm of Hoya U-340 filter. The absence of infrared-sensitive minerals (*e.g.* feldspars) was checked and confirmed using an infrared bleach provided by a solid state laser diode (830Δ10nm; 1W cm^2) at 50°C for 100 s before green-light stimulation. Laboratory doses used for constructing dose response curves were given using a calibrated $^{90}Sr/^{90}Y$ beta source housed within the reader. Multi-grain palaeodoses were determined from the first 2 s of OSL, using the final 10 s as background.

An instrumental reproducibility uncertainty of 2% was added (in quadrature) to each OSL measurement error. Single aliquot dose-response curves (SI Figure 14) were fitted using a saturating-exponential-plus-linear function using a weighted linear fitting procedure based on propagation of all measurement errors. Tests of protocol performance were made for thermal transfer and test-dose sensitivity correction, which returned thermally-transferred signals of <3% of the natural OSL at zero applied dose, and a mean 'recycling ratio' of 0.98 for duplicate regenerative doses. Measurements based on six aliquots provided a mean weighted palaeodose of 72.36 ± 4.99 Gy (SI Figure 15).

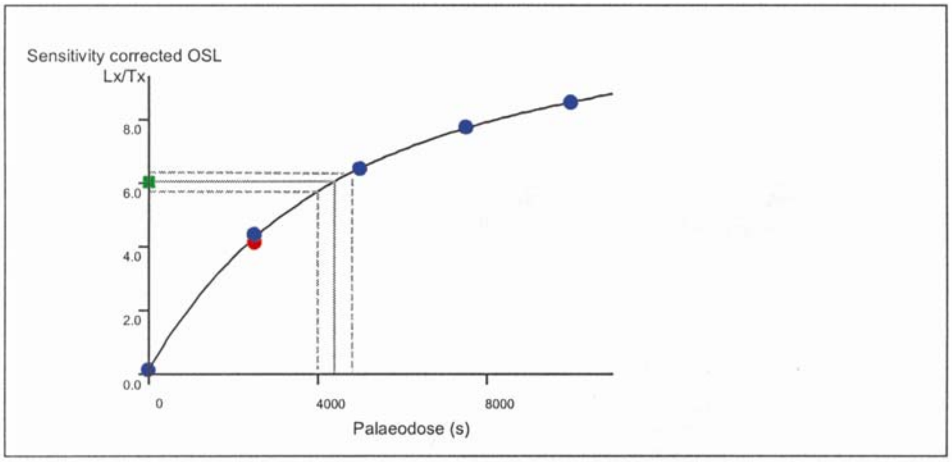

SI Figure 14. Single aliquot regenerative dose response curve for a quartz aliquot from sample X2509 (green square = natural OSL signal; blue circles = regeneration doses; red circle = repeated dose point).

To calculate the environmental dose rate, we combined the results of *in situ* γ-ray spectroscopy measurements with elemental analysis by inductively coupled plasma mass spectroscopy (ICP-MS) using a fusion sample preparation method. A portable γ-ray spectrometer (Ortec Micronomad multi channel analyser equipped with a 3x3 inch NaI (Tl) scintillator crystal) was employed in a 4 π-geometry and calibrated against the Oxford calibration blocks (15). Such on-site measurements provide direct estimation of the total γ-ray radiation field (≈30 cm radius sphere of the sampling location). Unfortunately, no readings could be acquired at the precise location of sample X2509 due to the hardness of the indurated sediment, which made it impossible to auger a suitable hole to insert the detector. Instead, the external gamma dose rate was derived from a spectrum obtained slightly higher up in the northern profile [layer 2b] and which provided a value of 0.458 Gy/ka.

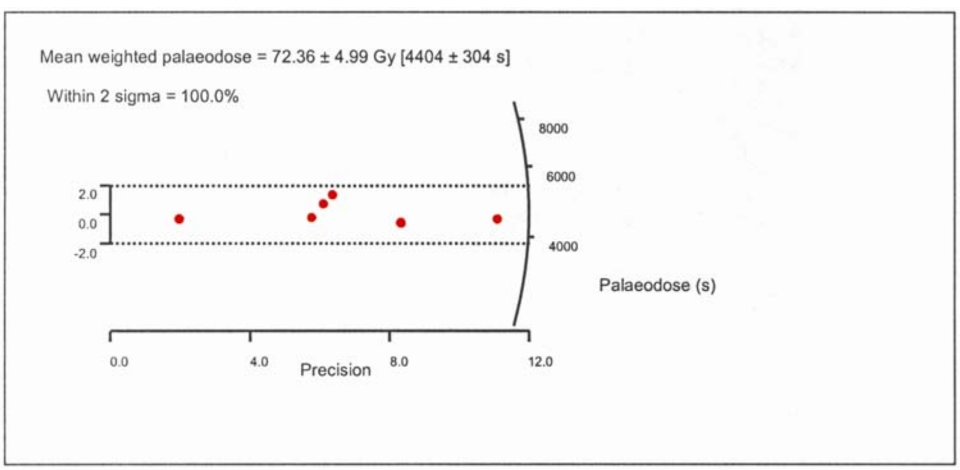

SI Figure 15. Radial plot of palaeodose values obtained for replicate aliquots from sample X2509.

The beta dose rate was derived from the concentrations of potassium (0.78%), thorium (3.7 ppm) and uranium (1.2 ppm) obtained by the laboratory-based ICP-MS analysis of the sediment. These values were converted to dose rates, making allowance for beta-dose attenuation and sample water content (16). Account was also taken of the cosmic-ray contribution (adjusted for site altitude, geomagnetic latitude, thickness of the cave roof, as well as thickness and water content of the sediment overburden) according to values provided by Prescott and Hutton (17). To calculate the optical ages, we assume that the measured radionuclide activities have prevailed throughout the period of sample burial and our calculations are based on an estimated mean field water content of 2-8% of the dry weight of the sediment. The total dose rate based on combined γ-ray spectroscopy measurements and ICP-MS analysis was 1.32 ± 0.06 Gy/ka. A slightly higher environmental dose rate of 1.38 Gy/ka is obtained if the calculations are solely based on the elemental analysis of the sedimentary matrix. Given the proximity of the OSL sample to a slab of marble, it seems more appropriate to use the lower dose rate value provided by the combination of field radioactivity measurements and laboratory-based ICP-MS analysis. The latter would not take into account the potential contribution of fragments of limestone and marble, which are present within the sedimentary units and which tend to have lower concentrations of radioisotopes. Based on the above premises, the calculated OSL age estimate for sample X2509 is 54.7 ± 4.7 ka cal BP.

Supporting Information VI:
Additional Data for the Palomas Human Remains

SI Table 4. Mandibular corpus breadths at the mental foramen for the Palomas mature mandibles and summary values for the comparative samples [mean ± SD (N)], in millimeters. The Neandertal sample includes Palomas 1, 6 and 23. MPMH: Middle Paleolithic modern humans; EUP: Early Upper Paleolithic humans; MUP: Middle Upper Paleolithic humans.

	Corpus Height at the Mental Foraman	**Corpus Breadth at the Mental Foramen**
Palomas 1	30.5	14.5
Palomas 6	27.0	15.7
Palomas 23	28.4	14.0
Palomas 59	26.4	12.8
Neandertals	32.1 ± 3.65 (31)	15.8 ± 1.6 (32)
MPMH	35.0, 36.0, 40.5	13.2, 15.0, 16.6
EUP	27.5, 33.2, 35.3	11.6, 12.2, 15.7
MUP	31.9 ± 4.1 (14)	12.7 ± 1.9 (13)

SI Table 5. Root lengths from the cervix to the root apex for mature teeth with complete closure for Palomas and the comparative sample teeth, in millimeters [mean ± SD (N), range]. Neandertal and Upper Paleolithic data from refs 18-20 and personal measurement. The Neandertal sample includes Palomas 1 and 24. Data are unavailable for the MPMH. Kruskal-Wallis (K-W) P-values are provided for comparisons across the three comparative samples.

	Palomas	**Neandertal**	**Early Upper Paleolithic**	**Middle Upper Paleolithic**	**K-W P-value**
Maxillary I^1		17.4 ± 1.4 (15)	13.8 ± 1.7 (5)	13.4 ± 1.8 (7)	<0.001
SP 24,79,90	15.5, 16.0, 16.4	15.7 – 20.1	11.7 – 16.5	11.0 – 16.3	
Maxillary I^2		17.1 ± 1.6 (14)	13.1, 17.0	14.7 ± 1.3 (4)	0.062
SP 43,48	20.4, 14.3	14.2 – 19.2		13.0 – 15.8	
Maxillary C^1		21.7 ± 2.6 (16)	16.0, 18.7, 23.0	16.0, 18.7, 23.0	0.021
SP 35,74	21.1, 18.1	15.6 – 26.2		12.5 – 19.7	
Mandibular I_1		17.3 ± 1.4 (9)	10.7, 13.7	13.9 ± 1.7 (8)	0.006
SP 19,21	15.0, 13.9	15.7 – 20.0		11.8 – 17.0	
Mandibular I_2		16.7 ± 1.1 (8	14.4 ± 1.8 (4)	14.5 ± 1.4 (7)	0.011
SP 20	16.8	15.0 – 17.9	11.8 – 15.5	12.4 – 16.4	
Mandibular C_1		21.0 ± 2.7 (14)	17.8 ± 0.8 (4)	15.7 ± 1.9 (6)	0.001
SP 18,26,44,82	18.2, 14.5, 21.9, 16.6	16.3 – 26.0	17.3 – 19.0	13.0 – 18.3	

SI Table 6. Labiolingual crown diameters for Palomas mandibular anterior teeth and summary values for the comparative samples [mean ± SD (N)], in millimeters. The Neandertal sample includes Palomas 1 and 89.

	I_1 Breadth	**I_2 Breadth**	**C_1 Breadth**
Palomas 1	6.8	7.2	9.0
Palomas 18			8.6
Palomas 19	7.0		
Palomas 20		6.8	
Palomas 21	6.6		
Palomas 26			7.6
Palomas 54			7.4
Palomas 59			7.3
Palomas 82			9.1
Palomas 89		7.2	
Palomas 91		7.8	
Neandertals	7.4 ± 0.4 (27)	7.8 ± 0.5 (41)	9.1 ± 0.7 (45)
MPMH	6.6 ± 0.6 (11)	7.1 ± 0.6 (10)	8.3 ± 0.8 (10)
EUP	6.9 ± 0.3 (5)	7.3 ± 0.5 (7)	8.8 ± 0.7 (7)
MUP	6.2 ± 0.4 (21)	6.8 ± 0.5 (22)	8.6 ± 0.7 (19)

SI Table 7. Manual distal phalanx 2-4 articular lengths and distal tuberosity breadth for Palomas 28 and summary values for the comparative samples [mean ± SD (N)], in millimeters. There are no known EUP distal manual phalanges. For the comparative samples, given uncetainty in assigning distal phalanges 2-4 to digit, available data are averaged by individual prior to sample summary statistic computations.

	Distal Phalanx 2-4 Articular Length	**Distal Phalanx 2-4 Distal Breadth**
Palomas 28	17.5	9.7
Neandertals	19.7 ± 1.5 (16)	10.4 ± 1.3 (11)
MPMH	18.6, 20.5, 20.6	7.7, 7.9, 8.2
MUP	17.4 ± 1.4 (11)	7.0 ± 1.4 (11)

Supporting Information References

1. Walker MJ (2001) in *A Very Remote Period Indeed*. eds Milliken S, Cook J (Oxbow, Oxford), pp 153-159.
2. DeNiro MJ (1985) Post-mortem preservation and alteration of *in vivo* bone collagen isotope ratios in relation to paleodietary reconstruction. *Nature* 317:806-809.
3. Hughen K, Southon J, Lehmanc S, Bertranda C, Turnbull J. 2006. Marine-derived ^{14}C calibration and activity record for the past 50,000 years updated from the Cariaco Basin. *Quatern Sci Rev* 25:3216–3227.
4. Fairbanks RG *et al*. (2005) Marine radiocarbon calibration curve spanning 0 to 50,000 years B.P. based on paired ^{230}Th/^{234}U/^{238}U and ^{14}C dates on pristine corals. *Quatern Sc Rev* 24:1781-1796 (http://www.radiocarbon.ldeo.columbia.edu/research/radcarbcal.htm).
5. Millard AR, Hedges REM (1996). A diffusion-adsorption model of uranium uptake by archaeological bone. *Geochim Cosmochim Acta* 60**:**2139-2152.
6. Pike AWG, Hedges REM, VanCalsteren P (2002). U-series dating of bone using the diffusion-adsorption model. *Geochim Cosmochim Acta* 66**:**4273-4286.
7. Pike AWG, Eggins S, Grün R, Thackeray F (2004) U-series dating of TP1, an almost complete human skeleton from Tuinplaas (Springbok Flats), South Africa**.** *S Afr J Sci* 100:381-383.
8. Pike AWG, Eggins S, Grün R, Hedges REM, Jacobi RM (2005) U-series dating of the Late Pleistocene fauna from Wood Quarry (Steetley), Notinghamshire, UK. *J Quatern Sci* 20:59-65.
9. Eggins SM *et al*. (2005) In situ U-series dating by laser ablation multi-collector ICPMS: new prospects for Quaternary geochronology. *Quatern Sci Rev* 24:2523-2538.
10. Huntley DJ, Godfrey-Smith DI, Thewalt MLW (1985) Optical dating of sediments. *Nature* 313:105–107.
11. Aitken MJ (1998) *An Introduction to Optical Dating* (Oxford University Press, Oxford).
12. Duller GAT (2004) Luminescence dating of Quaternary sediments: recent advances. *J Quatern Sci* 19:183-192.
13. Lian O, Roberts RG (2006) Dating the Quaternary: progress in luminescence dating of sediments. *Quatern Sci Rev* 25:2449-2468.
14. Murray AS, Wintle AG (2000) Luminescence dating of quartz using an improved single-aliquot regenerative-dose protocol. *Rad Meas*, 32:57-73.
15. Rhodes EJ, Schwenninger JL (2007) Dose rates and radioisotope concentrations in the concrete calibration blocks at Oxford. *Ancient TL* 25:5–8.
16. Adameic G, Aitken M (1998) Dose rate conversion factors: update. *Ancient TL* 16:37-50.
17. Prescott J R, Hutton JT (1994) Cosmic ray contributions to dose rates for luminescence and ESR dating: large depths and long-term time variations. *Rad Meas* 23:497–500.
18. Matiegka, J. (1934). *Homo předmostensis. Fosilní člověk z Předmostí na Moravě I. Lebky* (Česká Akademie Věd a Umění, Prague)
19. Vlček E (1969) *Neandertaler der Tschechoslowakei* (Academia Prag, Prague).
20. Bailey SE (2005) in *Current Trends in Dental Morphology Research*, ed Zadzinska E (University of Lodz Press, Lodz), pp 201–210.